

The colour of galaxies in distant groups

Michael L. Balogh¹, Sean L. McGee¹, Dave Wilman², Richard G. Bower³,
George Hau⁴, Simon L. Morris³, J. S. Mulchaey⁵, A. Oemler Jr.⁵, Laura Parker⁶,
Stephen Gwyn⁷

¹*Department of Physics and Astronomy, University of Waterloo, Waterloo, Ontario, N2L 3G1, Canada*

²*Max-Planck-Institut für extraterrestrische Physik, Giessenbachstrasse 85748 Garching Germany*

³*Department of Physics, University of Durham, Durham, UK, DH1 3LE*

⁴*Centre for Astrophysics and Supercomputing, Swinburne University of Technology, Hawthorn, Victoria 3122, Australia*

⁵*Observatories of the Carnegie Institution, 813 Santa Barbara Street, Pasadena, California, USA*

⁶*Department of Physics and Astronomy, McMaster University, Hamilton, Ontario, L8S 4M1 Canada*

⁷*Canadian Astronomical Data Centre, Herzberg Institute of Astrophysics Victoria, BC, Canada*

25 March 2022

ABSTRACT

We present new optical and near-infrared imaging for a sample of 98 spectroscopically-selected galaxy groups at $0.25 < z < 0.55$, most of which have velocity dispersions $\sigma < 500$ km/s. We use *psf*-matched aperture photometry to measure accurate colours for group members and the surrounding field population. The sample is statistically complete above a stellar mass limit of approximately $M = 1 \times 10^{10} M_{\odot}$. The overall colour distribution is bimodal in both the field and group samples; but at fixed luminosity the fraction of group galaxies populating the red peak is larger, by $\sim 20 \pm 7$ per cent, than that of the field. In particular, group members with early-type morphologies, as identified in *Hubble Space Telescope* imaging, exhibit a tight red sequence, similar to that seen for more massive clusters. Using optical and near-infrared colours, including data from the *Spitzer Space Telescope*, we show that approximately 20–30 per cent of galaxies on the red sequence may be dust-reddened galaxies with non-negligible star formation and early-spiral morphologies. This is true of both the field and group sample, and shows little dependence on near infrared luminosity. Thus, the fraction of bright ($^{0.4}M_K < -22$) group members with no sign of star formation or AGN activity, as identified by their colours or [OII] emission, is 54 ± 6 per cent. Our field sample, which includes galaxies in all environments, contains 35 ± 3 per cent of such inactive galaxies, consistent with the amount expected if *all* such galaxies are located in groups and clusters. This reinforces our earlier conclusions, that dense environments at $z \lesssim 0.5$ are associated with a premature cessation of star formation in some galaxies; in particular we find no evidence for significantly enhanced star formation in these environments. Simple galaxy formation models predict a quenching of star formation in groups that is too efficient, overpopulating the red sequence. Attempts to fix this by increasing the timescale of this quenching equally for all group members distorts the colour distribution in a way that is inconsistent with observations.

Key words: galaxies: clusters

1 INTRODUCTION

The evolution of the galaxy population since a redshift of about $z = 1$ appears to be a strong function of both stellar mass and environment (e.g. Juneau et al. 2005; Balogh et al. 2004a; Blanton et al. 2005; Baldry et al. 2006; Haines et al. 2006, 2008; van den Bosch et al. 2008; Gilbank & Balogh 2008; Cowie & Barger 2008). The overall effect is for star formation activity to decrease with time, with such activity apparently ceasing first in the most massive galaxies. Fundamentally, this evolution is linked to the accretion, radiative cooling, and reheating of

gas by individual galaxies (Bower et al. 2006; Croton et al. 2006; Dekel & Birnboim 2006; Somerville et al. 2008). But a wide variety of physical processes operating on an enormous range of scales may play important roles in how this gas component behaves, and we are still a long way from knowing which are most important on which scales, and at which epochs.

A particularly efficient way to track the evolution of star formation activity is through two- or three-colour optical photometry. Optical colours are almost equally sensitive to galaxy age, metal abundance, and dust content, which at first seems discour-

aging. To first order, however, the bulk of the galaxy population appears to be driven by only a few, correlated parameters. Most markedly, galaxies can be cleanly divided into two families — one red and one blue — that differ mostly in their star formation history (e.g. Strateva et al. 2001; Baldry et al. 2004); this distinction appears to hold to at least $z = 2$ (Bell et al. 2004; Gerke et al. 2007; Cassata et al. 2008). Within each of these families, there is a well-known correlation with magnitude (or stellar mass), that is at least partly driven by a systematic variation in metal content and possibly dust. The origin of the significant scatter about these correlations is not well understood, but almost certainly includes variation in all three parameters. In particular, it is known that the red population includes galaxies with significant amounts of star formation (e.g. Wilman et al. 2008; Wolf et al. 2009).

Making a few important assumptions, the stellar mass of a galaxy can be relatively easily measured from its luminosity. Using large-area redshift surveys and multicolour imaging (including the near-infrared) it has therefore become possible to study correlations of galaxy properties with mass, over a long redshift baseline (e.g. Cowie & Barger 2008). Although still a subject of debate, the role of mass or surface mass density as a driving factor of galaxy evolution is becoming clear (Taylor et al. 2009; Marchesini et al. 2008). The stellar mass functions of red and blue galaxies are distinct, and they also appear to evolve differently with redshift (e.g. Bell et al. 2007b). In particular, the most massive galaxies ($M \gtrsim 2 \times 10^{10} M_{\odot}$) today have predominantly old stellar populations, independent of environment (e.g. Kauffmann et al. 2003). It has been proposed that the supermassive black holes harboured within these galaxies can provide enough feedback energy to re-heat or expel the cooling gas necessary for star formation to occur (Birnboim & Dekel 2003; Croton et al. 2006; Bower et al. 2006; Dekel & Birnboim 2006; Sijacki et al. 2007). Although the giant galaxies found in clusters can sometimes show evidence for recent star formation, especially if they are located near the peak of an X-ray cool core (e.g. Crawford et al. 1999; Edwards et al. 2007; Bildfell et al. 2008; Rafferty et al. 2008), the associated star formation rates are still low relative to the galaxy’s mass (e.g. O’Dea et al. 2008).

On the other hand, the role of environment, if any, is still unclear. It is well known that dense environments today harbour less active galaxies, in general (e.g. Balogh et al. 1997; Lewis et al. 2002; Gomez et al. 2003; Blanton et al. 2005; Haines et al. 2006, and many others). That correlation is weakened somewhat when one accounts for the fact that denser environments contain more massive galaxies (e.g. Baldry et al. 2006), but it still persists; in fact, the data show that environmental effects are most easily observed in the low-mass galaxy population (e.g. Baldry et al. 2006; van den Bosch et al. 2008).

In principle, the evolution of galaxies in dense environments can be observed directly by comparing samples at different redshift. This is complicated however by the hierarchical growth of structure, which means that galaxies within clusters today were found within systems spanning a wide range of lower masses at higher redshift (e.g. Berrier et al. 2009; McGee et al. 2009). Locally, the properties of galaxies at fixed stellar mass show little or no dependence on the mass of the group or cluster in which they reside, at least for systems with velocity dispersions $\sigma > 500$ km/s (e.g. Balogh et al. 2004b; Weinmann et al. 2006a; Poggianti et al. 2006, 2008; Finn et al. 2008; Pasquali et al. 2009). These massive systems also appear to evolve little with redshift, at least for $z \lesssim 1$ (e.g. Nakata et al. 2005; Pasquali et al. 2009). On the other hand, lower-mass groups may be generally more active at higher

redshift (e.g. Poggianti et al. 2008), though always less so than the general field (e.g. Wilman et al. 2005b; Jeltema et al. 2007). If these intermediate redshift groups at $z \sim 0.5$ are to evolve into more massive clusters by the present day, this implies that there is a mechanism for truncating star formation in systems with halo masses approximately corresponding to those of small galaxy groups (Gilbank & Balogh 2008). At even higher redshifts, $z \sim 1$, although dense environments still contain a higher frequency of evolved galaxies, those that *are* active in groups and clusters may have greater star formation rates than the field, implying that local interactions may be more important than the global environment (e.g. Cooper et al. 2006, 2008; Elbaz et al. 2007; Muzzin et al. 2008).

The simplest model for environmental effects that has shown some success is one where satellite galaxies (those not at the centre of the potential) are immediately stripped of all hot gas (e.g. White & Frenk 1991; Cole et al. 2000). This, coupled with fairly short gas consumption and ejection timescales, leads to rapid truncation times, and satellite populations that are uniformly red at the present day (Croton et al. 2006; Bower et al. 2006). However, some observations suggest that the quenching is a more gradual process (e.g. Balogh et al. 1999, 2000; Moran et al. 2006; Gallazzi et al. 2009; McGee et al. 2008, 2009). One clue to why this might be is that some active galaxies in dense environments exhibit truncated or distorted H α disks, implying that star formation is truncated first in the outskirts of the galaxies (e.g. Koopmann & Kenney 2004; Bamford et al. 2007), rather than all at once. The result is that nearby observed groups and clusters tend to have many more blue, active low-mass galaxies than are predicted by this simple gas stripping model (Weinmann et al. 2006b; Baldry et al. 2006; Gilbank & Balogh 2008; Font et al. 2008).

The observations above suggest that galaxy groups at $z \approx 0.5$ may represent a critical environment for galaxy evolution. We have therefore embarked on an ambitious programme to obtain a complete census of the galaxy population in these environments. Our survey is based on the CNOC2 redshift survey (Yee et al. 2000), as described in Wilman et al. (2005a) and Carlberg et al. (2001a). In a series of papers we have shown that the galaxies in these groups do not differ strongly from the surrounding field, except that they have a slightly larger fraction of passively-evolving, bulge-dominated galaxies (Wilman et al. 2005b; Balogh et al. 2007; Wilman et al. 2008; McGee et al. 2008). However, these works were hampered by the relatively poor quality of the original optical imaging of the CNOC2 survey. Here we present improved optical imaging, in the *ugrizBVRI* filters from the CFHT Megacam and CFH12K imagers. These are combined with our ground-based and *Spitzer* IRAC near-infrared (NIR) photometry (Balogh et al. 2007; Wilman et al. 2008), including new K_s observations from the New Technology Telescope (NTT).

We describe the survey data in § 2, including a summary of the original survey observations and our follow-up spectroscopy. The analysis of the new imaging data is presented in § 3. The results are described in § 4, and discussed in § 5. Our conclusions follow, in § 6. For all cosmology-dependent calculations, we assume $\Omega_m = 0.3$, $\Omega_{\Lambda} = 0.7$ and $h = 0.7$. All magnitudes are in the AB system unless otherwise noted.

2 THE DATA

The original CNOC2 redshift survey consists of four widely separated fields, at approximate RA positions of 2h, 9h, 14h and 21h.

Each patch was surveyed with a mosaic of several $9.3' \times 8.3'$ CFHT-MOS fields, in an unusual and somewhat awkward geometry, consisting of a main square (3×3 MOS fields) area, and two or three linear extensions (Yee et al. 2000). Medium-resolution optical spectroscopy was obtained for ~ 6000 galaxies in these fields; target selection was based only on R_c magnitude, and the spectroscopic completeness is 50 per cent at magnitudes brighter than $R_c = 21.5$. From these data, Carlberg et al. (2001b) identified several hundred groups over the redshift range $0.1 < z < 0.55$, using a redshift-space friends-of-friends algorithm with the additional criterion that the local overdensity be positive. We used the multi-object spectrograph LDSS2 on the 6.5-m Baade telescope at Las Campanas Observatory in Chile to obtain a deeper and more complete sample of galaxies in the region of twenty-six of these groups at $0.3 \leq z \leq 0.55$ (Wilman et al. 2005a). We selected galaxies from the original MOS imaging, and obtained 418 additional redshifts, of which 240 are in the range $21 \leq R_c \leq 22$ and 86 are confirmed members of identified groups. The result is a 74 per cent completeness for $R_c < 22$, with well-understood selection functions (that depend almost entirely on R_c magnitude and geometrical position) as described in Wilman et al. (2005a). The original CNOC2 spectra span a wavelength range $4387\text{--}6285\text{\AA}$ due to use of a band-limiting filter, while our follow-up Magellan spectra cover the full optical range $3700\text{--}8000\text{\AA}$. The redshifts have a typical uncertainty of 100 km/s from the original survey, and 140 km/s in our follow-up spectroscopy.

In this paper we present *psf*-matched aperture photometry at optical and near-infrared wavelengths, for galaxies with redshifts in the four CNOC2 survey fields. Most of the follow-up data we consider here is centred on the $25' \times 25'$ contiguous central region, and coverage of the “extensions” is more limited. The images considered here come from a mixture of proprietary and archive data: *ugriz* and *BVRI* from the Canada–France–Hawaii Telescope; K_s from the William Herschel Telescope and the New Technology Telescope; and $3.6\mu\text{m}$ and $8\mu\text{m}$ images from *Spitzer Space Telescope*. These data and their processing are described in more detail below.

2.1 Optical imaging

The original redshift survey was based on relatively poor quality MOS imaging. Although perfectly acceptable for the spectroscopic selection that was the focus of the original survey, statistical and systematic uncertainties on the order of ~ 0.1 mag make it difficult to cleanly identify distinct galaxy populations from their optical colours (for example, see Figure 10 in Balogh et al. 2007). Therefore, we have obtained additional optical imaging from two wide-field mosaic cameras on the CFHT: the CFH12K and Megacam.

We also use data from the Advanced Camera for Surveys (ACS) on the *Hubble Space Telescope*. These data, described in McGee et al. (2008), consist of 20 ACS fields in the F775W filter. We will use the morphological measurements from these data, as described in Wilman et al. (2009), but not the photometry.

2.1.1 CFH12K images

The CFH12K is the previous generation large imager on the CFHT, with 12 close-packed 2048×4096 pixel CCDs, covering 42×28 arcmin with $0.206''$ pixels. We obtained most of these images from the CADC archive, and they were subsequently processed and

stacked as described below. The exceptions are the I-band images in the 14h and 21h patches, which were obtained and reduced as described in Parker et al. (2005). Although some of the patches have multiple pointings, covering a wider field, we only consider the single CFH12K pointing near the centre of each CNOC2 patch; dithering increases the coverage by a few arcmin in each dimension. All four patches have coverage in all four filters, *BVRI*.

Individual exposure times are typically 540–840s, depending on the filter; the total exposure times of the stacked images, and the characteristic full-width at half maximum (fwhm) of the seeing, are given in Table 1. Individual frames were dithered so the stacked frames suitably fill in all chip gaps. The ELIXIR¹ pipeline-processed data available from the CFHT archive were not directly usable, as there are zeropoint shifts remaining from chip to chip that are not correctly accounted for. These shifts appear to be constant for a given run, so it was possible to correct by comparing with overlapping Sloan Digital Sky Survey (SDSS) data, where available. However, there remains small-scale background variation which affects photometry at the 0.03 mag level. The only fringe correction is done on the individual images by the ELIXIR pipeline.

Those images overlapping with SDSS were calibrated by converting SDSS magnitudes of stars to CFH12K magnitudes using the following empirical conversions:

$$B = g + 0.4289(g - r) \quad (1)$$

$$V = g - 0.5561(g - r) + 0.0720(r - i) \quad (2)$$

$$R = r - 0.2178(r - i) - 0.0327(g - r) \quad (3)$$

$$I = i - 0.4451(i - z) \quad (4)$$

$$Z = z - 0.1682(i - z). \quad (5)$$

These conversions have a scatter of typically 0.01 mag (0.04 mag for *B*). Stars in SDSS are thus transformed on to the CFH12K system, and the images are calibrated against this sample. As the 21h field does not overlap with the SDSS, we calibrated the photometry by comparing with both Hsieh et al. (2005) and the original CNOC2 MOS photometry (Yee et al. 2000). The zeropoints calibrated in this way are accurate to approximately 0.03 mags.

The 14h and 21h field I band images are considerably deeper, and were processed and stacked as described in Parker et al. (2005).

2.1.2 Megacam images

Public archival Megacam images in *griz* were found in the CADC archive, and processed with MEGAPIPE (Gwyn 2008). Only the *i* image for the 21h field was not public at the time this work was done, and is therefore not included here. These are shorter (5–10 min) exposures than the CFH12K data, but cover a wider field and have a more accurate photometric and astrometric solution. However, as there are often only single pointings available, there are significant chip gaps which limit our coverage.

The *u* band data were obtained by us in semesters 2005A/B, for all patches except the 9h field. There were two sets of three dithered images for each of the three pointings; however, the dither pattern was not large enough to completely fill all the chip gaps. Each image was processed by the *Elixir* v.2.0 pipeline, which detrends each of the 36 chips. This process includes overscan, bias, masking and flat-fielding. Only data taken under photometric con-

¹ <http://www.cfht.hawaii.edu/Instruments/Elixir/home.html>

Patch	RA (J2000)	Dec (J2000)	Instrument	Filter	Total Exposure (ks)	Seeing (arcsec)
2h	02:26:03.906	+00:19:34.69	CFH12K	B	11.82	0.83
				V	2.65	0.75
				R	1.8	0.64
				I	1.8	0.55
			Megacam	u	13.97	0.80
				g	0.24	0.75
				r	0.48	0.66
				i	0.50	0.53
9h	09:23:46.657	+37:05:23.32	CFH12K	B	12.96	0.82
				V	6.0	1.01
				R	19.08	0.82
				I	5.16	0.89
			Megacam	g	0.24	0.83
				r	0.48	0.78
				i	1.05	1.20
				z	0.36	0.66
14h	14:49:38.084	+09:08:57.62	CFH12K	B	3.6	0.85
				V	3.6	0.94
				R	3.6	1.04
				I	14.4	0.75
			Megacam	u	16.64	0.80
				g	0.48	1.02
				r	0.96	0.91
				i	1.55	0.73
21h	21:51:20.350	-05:33:26.77	CFH12K	B	7.08	0.78
				V	7.44	0.76
				R	6.0	0.70
				I	14.4	0.68
			Megacam	u	14.72	0.80
				g	0.744	0.76
				r	0.528	0.69
				z	0.396	0.63

Table 1. Optical observations obtained from the CFHT archive.

ditions were combined, using the SWARP software provided by Terapix². The combined, final exposure times are listed in Table 1.

2.2 Near-infrared data

Near-infrared observations of these fields have been published by us in Balogh et al. (2007). Here we summarize these data, and include newer data obtained from the NTT. For this paper, all of these 2MASS-calibrated magnitudes were converted to the AB system by adding 1.85.

2.2.1 WHT INGRID observations

Our first infrared data in these fields were obtained at the *William Herschel Telescope* in March 2001, using the INGRID instrument. Good data were obtained for 23 $4.5' \times 4.5'$ fields centred on optically-detected galaxy groups in the 14h and 9h patches, with total exposure times of about 12 minutes per field. The data were reduced using the IPIPE NIR reduction pipeline (Gilbank et al. 2003),

as described in Balogh et al. (2007)³. Our magnitude zeropoints (on the Vega system) and astrometric solution were calibrated using the Two Micron All Sky Survey (2MASS; see Jarrett et al. 2000) point-source catalog K_s -band $4''$ standard aperture magnitudes. Due to the small field size, the photometric calibration is generally based on only a few (1-3) bright stars, and this dominates our uncertainties. The seeing for all 23 fields is better than $1''$.

2.2.2 Spitzer IRAC

Space-based NIR data from *Spitzer* IRAC was obtained from the archive, for the 2h, 9h and 14h fields. We used the processed $3.6\mu\text{m}$ and $8\mu\text{m}$ data directly from the archive, with no further reduction. These images cover a relatively large area, of $36.6' \times 43.6'$. However, they still do not generally cover the entire CNOC2 survey area. These data were also used and described in Balogh et al. (2007) and Wilman et al. (2008).

² <http://terapix.iap.fr/>

³ Small zeropoint adjustments have been made to three of the images since that work.

2.2.3 *NTT SOFI observations*

New data were obtained for 27 $6.9' \times 6.9'$ fields in the 2h, 14 and 21h patches, using the SOFI instrument⁴ on the *NTT*, using both service mode (period 76) and visitor mode (period 77). Data were reduced with the *NTT* observatory pipeline. An approximately 1 per cent gradient in the sky background following dome flat fielding was corrected using an illumination correction. The image scale is 0.288 arcsec per pixel, and the gain/readnoise are 5.4 and $11.34e^-$, respectively. Fields were typically observed with 24–36 separate exposures which were then combined using the pipeline software, for a total integration time of about 1 hour per field. In some cases, better results were obtained by combining subsets of the data first, and then coadding them after reduction. The astrometric solution was calculated based on the CFHT Megacam imaging where available. Outside the Megacam fields, either the ACS or original CNOC2 astrometry was used.

The service mode run also includes short, photometric exposures; however the visitor data was mostly obtained in nonphotometric conditions. In all cases, zeropoints were obtained by calibrating with the 2MASS point source catalogue. For the photometric observations taken in service mode, we find this gives zeropoints for a given run that are consistent to within 0.1 mag. This is limited by the small number of stars in each field, and the shallow depth of the 2MASS data. Comparing the SOFI and INGRID data for the few cases where there is some overlap in sources, the *rms* of the magnitude difference is ~ 0.2 mag, implying the INGRID zeropoint uncertainty is ~ 0.17 mag.

3 ANALYSIS

3.1 Object Detection and Photometry

Our primary goal is to obtain accurate colours for the galaxies in the original CNOC2 survey with $R < 22$, for which statistically complete spectroscopy exists. Our optical and near-infrared images are generally much deeper than this.

Object detection was done on a combined image of *R* (CFH12K) and *r* (Megacam). We used SWARP to align and combine these images into a single, large “super” image, using the LANCZOS3 resampling option and an Aitoff projection. The advantages of using this image for object detection are that the filter choice is close to that used in the original CNOC2 survey selection, we achieve maximum depth by combining the images, and we maximize continuity in the central regions (since the Megacam data alone contains chip gaps). The disadvantage is that the detection limit is non-uniform; however, as this is well below our limit of interest it is not a concern. We note that this approach also means there are survey regions with spectroscopy and good data in other filters (particularly the near-infrared) that are not included in our catalogues because they do not have Megacam-*r* or CFH12K-*R* coverage.

All the other data, including the NIR and *Spitzer* images, were aligned to this “super” image. For the INGRID and SOFI data, we combine all the individual, sky-subtracted images within a given patch, thus making a large image of mostly empty pixels, with small regions of data.

To measure accurate colours, we require all the images to be

matched in psf size. To make optimal use of the data, this requires two different data sets:

Optical/IR (OIR): For the optical and ground-based NIR imaging alone, the seeing is almost always better than $1''$; the only major exception is the 9h Megacam *i* image, with 1.2 arcsec seeing. Therefore, we convolve all of these data with an appropriate Gaussian to achieve $1''$ resolution.

OIR+IRAC: The IRAC data at 3.6 and 8 microns has a psf of approximately $2.3''$, limited by the $1.2''$ pixel size. Thus, whenever these data are used, colours must be measured in larger apertures and with a different psf correction. To achieve this, we generate a second set of optical/IR images smoothed to $2.3''$ seeing.

Photometry was performed with SEXTRACTOR v2.5 (Bertin & Arnouts 1996), in two image mode, where the “super” *r*-band image is always used for detection. This ensures that the same centres are used for photometry in all filters, and that both catalogues contain exactly the same objects, in the same order. RMS weight maps are used for both the detection and measurement images. Object detection is done using a $3''$ Gaussian kernel, and we require 3 pixels above the 1σ threshold. Deblending is performed with 32 sub-thresholds and a minimum contrast of 0.002. These parameters were chosen to provide the best results above $R = 22$, where we are most interested.

Aperture photometry is performed using a local background annulus, $10''$ thick. We use $3''$ diameter apertures for the OIR catalogues (which are smoothed to $1''$) and $5''$ apertures for the OIR+IRAC catalogues (smoothed to 2.3 arcsec). In this paper, we always use the best (i.e. highest resolution) colour when available. Colours are always computed using comparable magnitudes (i.e., measured on images of the same resolution and using the same aperture sizes). We have verified that there is no systematic bias between colours measured in (e.g.) $3''$ and $5''$ apertures, only increased scatter in the latter. Therefore, we will interchangeably use colours computed in different ways, as necessary. For example, (*r* – *i*) colours will be based on the $5''$ aperture colours for the 9h field (driven by the poor seeing of the *i* images), but $3''$ apertures for the others. There are obvious disadvantages to using fixed-aperture colours. One is that colours are not measured within consistent fractions of the effective radius, so in the presence of gradients we could be introducing a systematic error with galaxy size. However, we see no trend in the difference between $3''$ and $5''$ apertures with total luminosity, and conclude that this effect is small compared with our statistical uncertainties. The other disadvantage is that colours will be incorrect for close pairs of galaxies, but these represent a relatively small fraction of our sample with $r < 22$. Thus, we conclude that fixed-aperture colours are well-suited to our purpose of identifying the main variations in galaxy population with environment and redshift.

For total magnitudes, we use the SEXTRACTOR MAG_AUTO parameter, computed in the *R* or *r* band (CFH12K or Megacam). This is an elliptical-aperture measurement, with the aperture size based on the first moment of the object light distribution, with an automatic correction for neighbour contamination (we use the MASK_TYPE CORRECT option). This is the only total magnitude we compute directly. Total magnitudes in other filters are always derived from these, using the appropriate aperture colours.

Finally, the catalogues are matched to the CNOC2 redshift catalogues (including additional redshifts from our Magellan programme). Although the relative astrometry of each MOS field in the original CNOC2 survey is good, the global astrometric solution for each patch has significant offsets which makes matching sources difficult. Therefore we first improve upon the CNOC2 astrome-

⁴ Based on observing program 076.A.0346 and 077.A.0224.

try by re-solving each MOS pointing, using the publicly available ASTROMETRY.NET software (Hogg et al. 2008; Lang et al. 2009). This provides more accurate coordinates for all CNOC2 galaxies, and we then match them with the closest source in our new optical and infrared catalogues.

3.1.1 *K-corrections*

We compute *k*-corrections for all galaxies with redshifts, using the KCORRECT v4.1.4 software of Blanton & Roweis (2007). We use the 3'' aperture magnitudes, in *ugrizBVRiK* where available. We do not include the Spitzer data here, as it is not critical for *k*-corrections and would require us to use degraded (i.e. lower resolution) optical data for the psf-matched photometry. In the few cases where K_s imaging exists from both SOFI and INGRID, we take the SOFI value. For the optical photometry, we use the native systems and use the appropriate filter and instrument response curves. Since the K_s data were calibrated to 2MASS, we use the standard 2MASS response curves for these fluxes (and convert to the AB system). Magnitudes were corrected for Galactic extinction using the Schlegel et al. (1998) maps, where we have taken a single typical value for each CNOC2 patch⁵. A systematic calibration uncertainty was added in quadrature to the uncertainty computed by SExtractor. This was typically 0.02-0.03 for the optical filters, but 0.05 in *u* and K_s . Finally, we only fit galaxies with coverage in at least four different filters.

For this paper we *k*-correct the magnitudes to $z = 0.4$, to minimize the size of this correction. No evolution correction is applied. Thus, throughout this paper we always quote magnitudes corrected to the $z = 0.4$ observed frame, indicated by a superscript; for example, $^{0.4}r$ represents the observed *r* magnitude at $z = 0.4$.

Figure 1 shows the observed (*g-r*) colour as a function of redshift, for all galaxies with *k*-corrections. The points are colour-coded according to their $z = 0.4$ colour, as indicated. The fact that the points are properly segregated at all redshifts is one demonstration that the *k*-corrections we compute are reliable (e.g., the galaxies with the reddest $z = 0.4$ -frame colours are generally the reddest in observed colour at other redshifts). Although for some fits the reduced χ^2 value is large, we find no tendency for these *k*-corrections to be distributed differently as a function of colour and redshift than those with good fits. Therefore, we only omit data where there are fewer than four available filters, which would be of limited use to us here anyway.

Absolute magnitudes are computed from extinction and *k*-corrected magnitudes at $z = 0.4$, assuming $\Omega_m = 0.3$, $\Omega_\Lambda = 0.7$ and $h = 0.7$ as usual.

3.1.2 *Combining similar filters*

We will combine the photometry from different instruments, when the bandpasses are similar. By directly comparing galaxies in the relevant magnitude range with both CFH12K and Megacam coverage (approximately 200–350, depending on the filter), we compute the following transformations (lower-case filters refer to Megacam,

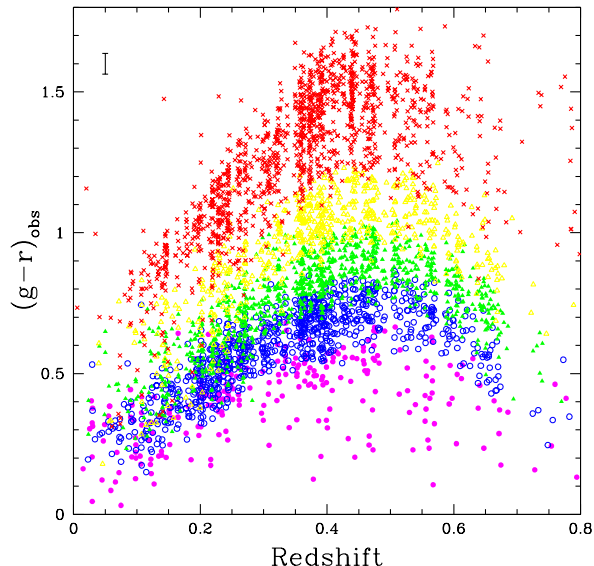


Figure 1. The observed Megacam (*g-r*) colours as a function of redshift, colour-coded according to their $z = 0.4$ frame colours. The filled, magenta circles represent galaxies with $^{0.4}(g-r) < 0.6$, and the blue, green, yellow and red symbols (open circles, filled and open triangles, and crosses, respectively) represent increasingly red bins in $z = 0.4$ colour, 0.2 mag wide. The error-bar in the top-left corner shows the typical 1σ uncertainty, including zeropoint error, for $r < 22.5$ galaxies at $0.25 < z < 0.55$.

while upper-case filters are CFH12K):

$$g = B + 0.058 - 0.588(B - V), \quad (6)$$

$$r = R - 0.07 + 0.261(V - R), \quad (7)$$

$$i = I + 0.119 \quad \text{if } (B - V) > 1, \quad (8)$$

$$i = I - 0.11 + 0.2(B - V) \quad \text{if } (B - V) \leq 1. \quad (9)$$

These transformations have an *rms* dispersion of 0.05 mag in *i* and *r*, and 0.08 mag in *g*.

In all cases, we will use the Megacam *gri* magnitudes if available; otherwise we will use the CFH12K *BRI* magnitudes, appropriately transformed using these relations.

It is also useful to combine the INGRID, SOFI and IRAC 3.6 μ m data into a single equivalent K_s band magnitude. This is trivial for the INGRID and SOFI data, since they are both calibrated to the 2MASS system. Although the 3.6 μ m data is obviously distinct from K_s , the relative insensitivity of this part of the spectrum to spectral type makes a simple conversion to K_s magnitudes a sensible thing to do for our purposes. We follow a strategy similar to that outlined in Balogh et al. (2007), noting that the [3.6]- K_s colour is primarily sensitive to redshift, as shown in Figure 2. This relationship has little dependence on intrinsic galaxy colour, and is similar whether we use SOFI or INGRID magnitudes, demonstrating indirectly that there is no systematic shift between their respective zeropoints. We fit this relationship with a constant value for $z < 0.35$, and a straight line at higher redshift, as shown. We use this fit to convert all [3.6] micron magnitudes to an equivalent K_s magnitude at that redshift, then apply the *k*-correction (to $z = 0.4$) computed for the K_s filter. Comparing galaxies with both ground-IR and IRAC data, we find an *rms* dispersion in this equivalent K_s (*AB*) magnitude of about 0.22 mag, which primarily reflects uncertainty in the ground-based zeropoint (about 0.1 mag) and a small residual colour term (also about 0.1 mag). The val-

⁵ Specifically, we model the extinction as $A_\lambda = A_o - 1.5 \log_{10} \lambda / \mu\text{m}$, with $A_o = -1.415$ in the 14h and 21h patches, $A_o = -1.285$ for the 2h patch, and $A_o = -1.8$ for the 9h patch.

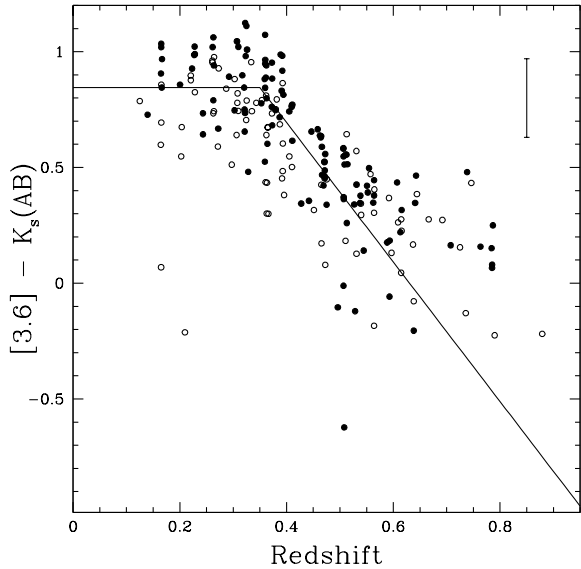


Figure 2. The observed $[3.6]-K_s$ colours as a function of redshift, for galaxies with $K_s < 20$, shows a fairly well-defined relation with rms scatter of about 0.22 mag. The error-bar in the top-left corner shows the typical 1σ uncertainty, including zeropoint error; this accounts for most of the scatter. There is little dependence on star formation history: the filled circles indicate galaxies with red colours, $^{0.4}(g-r) > 1.2$. The solid line shows a bilinear fit to this relation; we use this to convert $[3.6]$ magnitudes to equivalent AB K_s magnitudes at the appropriate redshift, then apply a k-correction to $z = 0.4$, as in Balogh et al. (2007). This allows us to treat the ground-based and space-based near-infrared measurements together.

ues of $K_s(AB)$ in this paper will always use the IRAC data where available, otherwise the SOFI or INGRID (in that order).

3.2 Group and field definition

We use the group centres and velocity dispersions as described in McGee et al. (2008), based on a slight modification of the method in Wilman et al. (2005a). Group members are considered to be all galaxies within 500 kpc of the luminosity-weighted centre, and within twice the group velocity dispersion in redshift. If there are two groups potentially satisfying these criteria for a given galaxy, the galaxy is assigned to the group to which it is closer spatially. Typical groups include ~ 10 confirmed members, and velocity dispersions are formally determined to within ± 100 km/s, using the gapper algorithm of Beers et al. (1990).

Figure 3 shows, as a function of group redshift, the distribution of σ_{rest} , the rest-frame velocity dispersion of the host group for each galaxy in our sample with $0.25 < z < 0.55$. These velocity dispersions are actually upper limits, as they include intrinsic dispersion due to redshift uncertainties. Most of the galaxies come from groups with $\sigma < 500$ km/s; in Balogh et al. (2007) we show that the stellar masses and lensing masses of these groups are also in good agreement with these velocity dispersions. Thus, our sample is dominated by true groups, and none of our results are changed if we exclude groups with $\sigma > 500$ km/s. The figure also shows which groups have optical, near-infrared and *HST* follow-up imaging, as described in the caption. We see that the subsample of groups considered in this paper is representative of our full group sample.

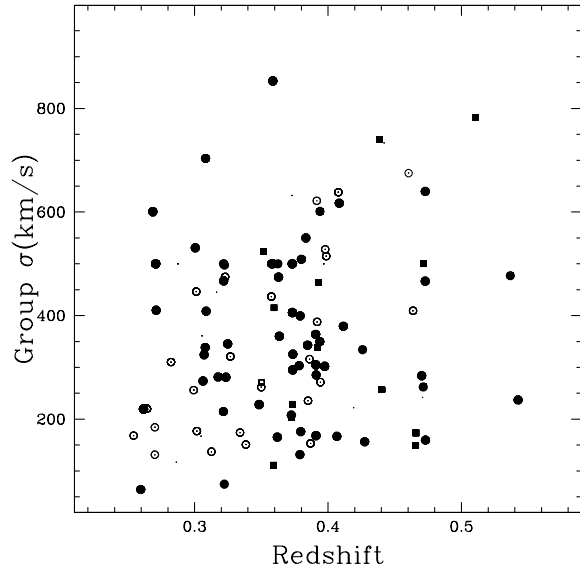


Figure 3. The rest-frame velocity dispersion of all groups in our sample is shown as a function of group redshift. Error bars are not shown, for clarity, but are typically ± 100 km/s. Filled symbols represent groups with near-infrared imaging, as described in § 2.2. Squares are groups with *HST* coverage (§ 3.5), while circles are those without. Small points are groups without new optical imaging from CFHT, and are excluded from all analysis in this paper.

We will define our field sample to be all galaxies in the survey that are not assigned to a group, either using our current definition or with the more encompassing friends-of-friends definition employed in previous papers. However, our group sample is not complete, partly because they were selected from a sparsely-sampled redshift survey (McGee et al. 2008). Therefore our field sample is more representative of the total galaxy population; we expect that approximately half of all galaxies in this sample are themselves in groups or clusters (Eke et al. 2004; McGee et al. 2008, 2009).

3.3 Statistical weights and Completeness

Our spectroscopic selection function is complex because certain fields within the original CNOC2 survey area were retargetted with LDSS2 on Magellan, improving both the completeness and depth. Since the fields were chosen to contain groups, the selection function also depends on environment. In previous papers (e.g. Balogh et al. 2007; Wilman et al. 2005a, 2008) we have implemented different, complex weighting schemes to try and account for this as best as possible. These methods are never perfect, and rarely have any substantial influence on the results.

Here we adopt a slightly simpler scheme, and apply weights that depend only on the R magnitude (from the original MOS imaging on which the spectroscopic targets were selected) and their location inside or outside of our Magellan target fields. That is, for the regions observed at Magellan, we compute completeness as a function of R , for all galaxies with spectra in that field (including those from the original CNOC2 survey). We do the same for the regions not covered by Magellan. This then provides a statistically-complete sample to $R < 21.5$; the Magellan fields are statistically complete to about 0.5 mag fainter than this.

Our photometry is all much deeper than our spectroscopic

limit. We would like to consider galaxy properties as a function of the reddest-possible band, which provides the best tracer of stellar mass. Ideally this would be the K_s and $[3.6]\mu\text{m}$ band data; however, we have a larger sample if we use i , so in this paper we will present our data as a function of both magnitudes. In our redshift range of interest, $0.25 < z < 0.55$, the reddest galaxies have $(r - i) \sim 0.8$ and $(r - K_s) \sim 2.5$, so the spectroscopic limit $R = 21.5$ corresponds to $i \sim 20.7$ and $K_s \sim 19$. In $z = 0.4$ frame absolute magnitudes, at $0.25 < z < 0.55$, these limits are $-19.8 > {}^{0.4}M_i > -21.8$ and $-21.5 > {}^{0.4}M_{K_s} > -23.5$. We use a $1/V_{\text{max}}$ weight to construct a statistically complete volume-limited sample within this redshift range, with ${}^{0.4}M_i < -19.8$ and ${}^{0.4}M_{K_s} < -21.5$. Note that this volume weight gets very large (greater than 20) within about 0.2 mag of these limits, so we restrict most of our analysis to ${}^{0.4}M_i < -20.0$ or ${}^{0.4}M_{K_s} < -21.7$.

3.4 Measures of activity

In addition to the colours of interest here, we consider other measures of galaxy ‘‘activity’’. This includes the rest-frame equivalent width of the [OII] emission line, $W_{\circ}([OII])$. These were measured on all spectra as described in Whitaker (2005), using the same algorithm as that described in Balogh et al. (1997). We take $W_{\circ}([OII]) > 10\text{\AA}$ as a secure indication of activity (but do not distinguish between star formation and AGN).

We also use the k-corrected IRAC [8]–[3.6] micron colours in $5''$ apertures, where available, as a more sensitive probe of activity, as described in Wilman et al. (2008). Wilman et al. (2008) show that $f_8/f_{3.6} > 0.5$ is a good indicator of activity, since galaxies with brighter $8\mu\text{m}$ emission at this redshift tend to be dominated by PAH emission lines related to star formation, or continuum emission from AGN. We will adopt the same definition for passively-evolving galaxies here, $f_8/f_{3.6} > 0.5$ here. Although we measure the photometry somewhat differently from Wilman et al. (2008), this does not make a large enough difference to motivate a change in threshold.

3.5 Morphology

We use the galaxy morphologies presented in Wilman et al. (2009). The morphologies are based on *HST* ACS observations of a subset of our groups. The classifications onto the Revised Hubble Scheme were made independently by two of us (AO and JM). To simplify somewhat, we group E and E/S0 together into a single ‘‘E’’ class. Similarly, S0/E, S0 and S0/a will all be treated as ‘‘S0’’. Sa and Sb will be termed ‘‘early S’’, while Sc, Sd and Sm will be ‘‘late S’’. Any irregular galaxy, or those identified as merging or interacting, will all be considered ‘‘Irr/M’’. For these purposes, notes of peculiarity will be ignored.

3.6 Stellar mass

Previously (Balogh et al. 2007; Wilman et al. 2008) we presented stellar mass estimates for a subset of galaxies in the present sample, based on simple stellar population models, and we will soon publish more accurate values computed from fits to the full spectral energy distribution available to us, including GALEX data (McGee et al. in prep). In this paper however, we aim to compare the properties of group and field galaxies as directly as possible, thus restricting our analysis to quantities closely related to observables

(i.e., instrumental colours and magnitudes at $z = 0.4$). Nonetheless it is useful to be able to relate absolute magnitudes in the $z = 0.4$ frame colours to an approximate stellar mass for reference. For this purpose, we compute two Bruzual & Charlot (2003) models galaxies with a Chabrier (2003) initial mass function and metallicity $0.2Z_{\odot}$, as expected to be appropriate near the limit of our data. The first is a dust-free, single stellar population of age 8.0 Gyr (the time between $z = 5$ and $z = 0.4$), and the other assumes a constant star formation rate for the same duration, and includes 1 magnitude of dust extinction. In the first case, we find $M/{}^{0.4}L_{K_s} = 0.35$ and $M/{}^{0.4}L_i = 1.6$, while for the second (younger) model $M/{}^{0.4}L_{K_s} = 0.22$ and $M/{}^{0.4}L_i = 0.78$. Thus, star-forming galaxies are 0.8 mag brighter in I , and 0.5 mag brighter in K_s , than old galaxies with the same stellar mass.

Recall that our sample is statistically complete, for galaxies of all colour, at ${}^{0.4}M_i < -20$ and ${}^{0.4}M_{K_s} < -21.7$. Using the simple models above, our sample is complete, for all galaxy types with $M \gtrsim 1 \times 10^{10} M_{\odot}$ (I -selected), or $M \gtrsim 2 \times 10^{10} M_{\odot}$ (K_s -selected). Note that the bluest objects in our sample reach luminosities as faint as ${}^{0.4}M_{K_s} = -19$, which corresponds to a stellar mass of $M = 1.0 \times 10^9 M_{\odot}$. It will be interesting to compare the field and group populations of such low-mass, star forming galaxies — even though the corresponding old population is not represented.

4 RESULTS

4.1 Colour distributions

We begin by considering colours that span the age-sensitive 4000\AA break. At $z = 0.4$ (to which all our magnitudes are k-corrected), this is $(B - R)$ in the CFH12K images, and $(g - r)$ for Megacam. To make the maximum use of our data, we transform CFH12K magnitudes to the Megacam system, as described in § 3.1.2. There are 2215 galaxies in our redshift range with spectroscopy and good g , r and i magnitudes. Of these, 333 are group members.

In Figure 4 we show the ${}^{0.4}(g - r)$ colours as a function of ${}^{0.4}M_i$, for group and field members in our sample. The point symbols are keyed to galaxy morphology, for those with ACS imaging, as indicated. As expected, the elliptical galaxies follow a tight red sequence, in both environments, with few exceptions. This is generally true also of the S0 galaxies, though a few of these show blue colours. There are almost no late-type spirals on the red sequence.

The data are colour-coded according to their level of activity. Blue symbols are galaxies with either strong [OII] emission, or an infrared excess, as described in § 3.4. To be conservative, red-coloured points are only those for which IRAC colours are available, and for which there is no IR excess. These are likely to be truly passive galaxies; we can’t say the same about galaxies with weak or absent [OII], since our spectra have relatively low S/N and this line is relatively weakly sensitive to star formation.

Our best tracer of stellar mass is the near-infrared K_s magnitude, converted from *Spitzer* [3.6] magnitude if available, and otherwise taken from our SOFI and INGRID data. This results in a smaller sample of only 1429 galaxies (303 in groups) but is the least-sensitive to stellar population effects. Because of the weak colour-dependence of $M/{}^{0.4}L_{K_s}$, a 0.5 mag interval in ${}^{0.4}M_{K_s}$ corresponds to only a factor ~ 2 variation in stellar mass; thus our K_s -selected sample is reasonably close to a mass-selected sample. We show the ${}^{0.4}(g - r)$ colours as a function of ${}^{0.4}M_{K_s}$ in Figure 5. The same features are visible here, as in Figure 4; in particular, the majority of blue galaxies in our sample are low-mass, well below

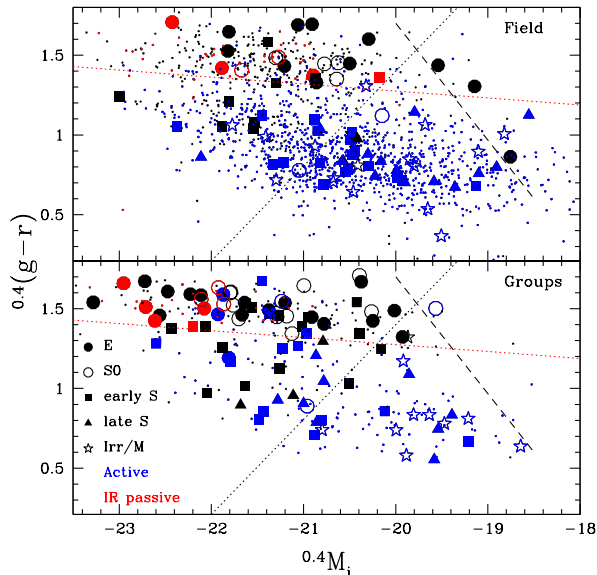


Figure 4. A colour-magnitude diagram for group galaxies (bottom panel) and field galaxies (top panel), in our $0.25 < z < 0.55$ sample. The large symbol types are keyed to galaxy morphology as described in § 3.5 and indicated in the legend; small circles have no ACS coverage, hence no morphological information. Blue symbols represent those galaxies that show either strong [OII] emission, or have an IR excess, indicating star formation or AGN activity. Red symbols are galaxies that show no IR excess. Black symbols are galaxies with no *Spitzer* data to measure an IR excess, and weak, absent or unmeasured [OII] emission. The black, dashed line shows our colour-dependent completeness limit at $z = 0.25$. Brighter than this there is absolute magnitude incompleteness, which we can correct with a V_{\max} weight. Fainter than $0.4M_i = -19.8$ the sample is incomplete for red galaxies. The black dotted line represents approximately a constant mass limit of $1 \times 10^{10} M_{\odot}$, computed by simply joining the young and old population synthesis models described in the text. The red dotted lines represent our division between red and blue galaxies, based on a 0.15 mag offset from a fit to the red sequence.

our colour-completeness limit of $\sim 2 \times 10^{10} M_{\odot}$, shown as the dotted black line in the figure. We emphasize that above this limit we have a statistically complete sample of group and field galaxies, independent of their colour. This should be compared with the higher redshift groups in the DEEP2 survey (e.g. Cooper et al. 2008), for which only the very most massive red galaxies are detected.

In Figure 6 we show the $0.4(g-r)$ colour distribution in four bins of infrared luminosity. Adopting an approximate $M/^{0.4}L_{K_s} = 0.3$, intermediate between the young and old models described in § 3.6, these bins are centred approximately on stellar masses of $1.2 \times 10^{11} M_{\odot}$, $6.3 \times 10^{10} M_{\odot}$, $3.5 \times 10^{10} M_{\odot}$ and $2.2 \times 10^{10} M_{\odot}$. The galaxies are weighted as described in § 3.3, including the V_{\max} weight. However, the group-member histograms are renormalized to the total number of galaxies in each luminosity bin, so the y-axis is more reflective of the unweighted sample size. The field histograms are normalized to match the number of group-galaxies in each bin, so the shapes can be directly compared.

This figure shows the now well-established bimodal distribution of galaxy colours. At all luminosities, the group sample shows more galaxies in the red part of the distribution than the corresponding field sample. Apart from that, the shape of the colour distribution looks remarkably similar for both environments. This also holds for lower-masses, where the sample is incomplete for red

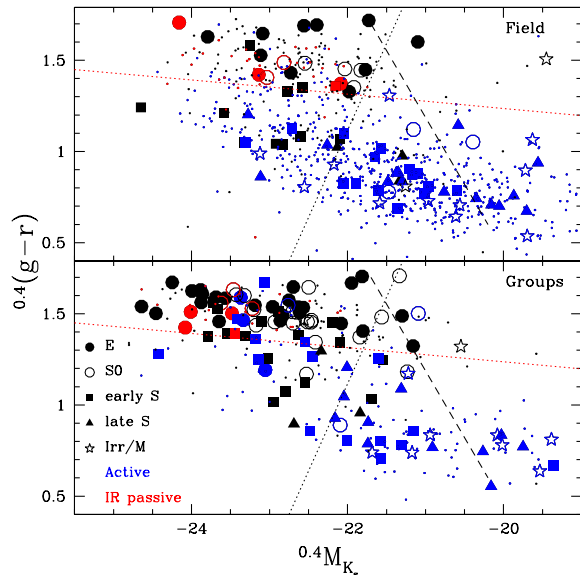


Figure 5. The same as Figure 4, but as a function of absolute K_s magnitude. Here, K_s is converted from *Spitzer* [3.6] micron fluxes if available; otherwise we use our SOFI and INGRID data. The black dotted line represents approximately a constant mass limit of $2 \times 10^{10} M_{\odot}$, computed by simply joining the young and old population synthesis models described in the text.

galaxies. The colour distribution of faint ($0.4M_{K_s} > -21$) galaxies along the blue sequence in the group sample is indistinguishable from that in the field, as apparent from Figure 5 and statistically confirmed with a K-S test.

Thus, as at low redshift, the dominant environmental effect observed is an increase in the fraction of red galaxies in dense environments. To quantify this, we fit a line to the red sequence and define a colour cut 0.15 mag bluer than this limit, as shown in Figures 4 and 5. We then compute the red fraction as a function of magnitude, weighting for incompleteness and volume effects as usual. The result is shown in Figure 7; error bars on weighted fractions, here and throughout the paper, are computed using binomial statistics (Gehrels 1986). At fixed luminosity, an additional $\sim 20 \pm 7$ per cent of the group population is found on the red sequence, compared with the field; this is true whether we use i or K_s luminosities, though the trend is weaker in the latter case. The well-known trend for lower-mass galaxies to have higher blue fractions (e.g. Baldry et al. 2006) holds equally well for our group galaxies. However, the key point here is that the galaxy population has a clear dependence on environment, independent of any trends with stellar mass.

4.2 Dusty red galaxies

The red sequence is known to include some actively star-forming galaxies that are reddened by dust (e.g. Wolf et al. 2005). At low redshift, these tend to be mostly early-type spiral galaxies with low star-formation rates, or highly-inclined normal spirals (Wolf et al. 2009). In Figure 8 we use a colour-colour diagram, with rest-frame colours chosen to be comparable to those in Wolf et al. (2005), to try and separate these populations. At $z = 0.4$, $(g-i)$ is an age-sensitive feature spanning the 4000Å break, while $(i-K_s)$ is more sensitive to dust. The field population in Figure 8 shows a clear ex-

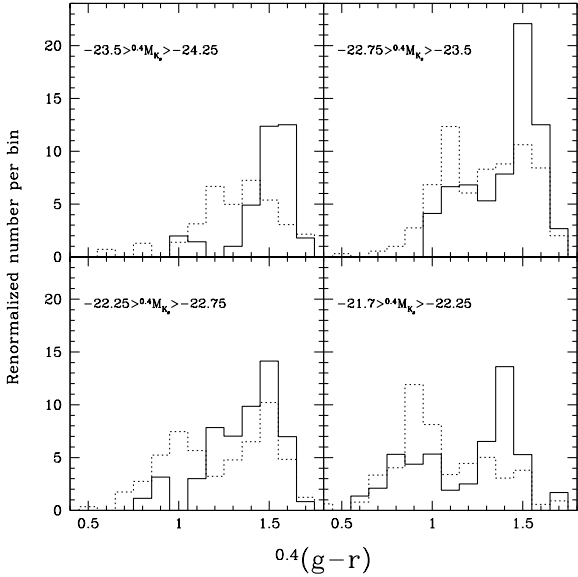


Figure 6. The colour distribution of galaxies in four near infrared luminosity bins, as indicated. Field galaxies are shown in dashed histograms, while group galaxies are shown with solid lines. Distributions are weighted by statistical sampling weights and $1/V_{\text{max}}$, but then renormalized to reflect the total number of *group* galaxies in each luminosity bin shown.

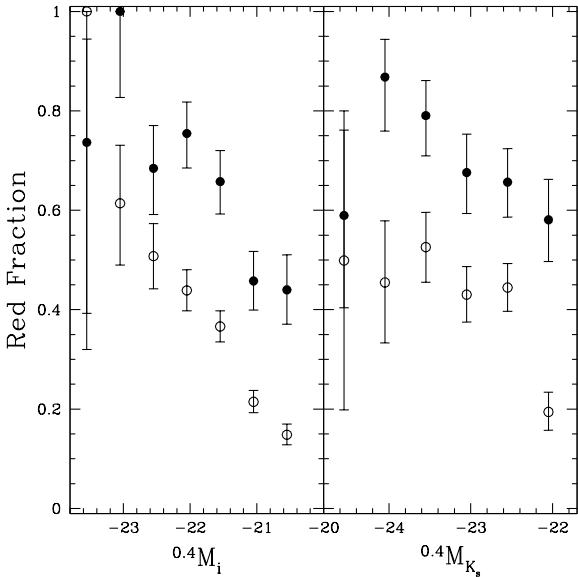


Figure 7. The fraction of red galaxies as a function of absolute magnitude, in the group (filled circles) and field (open circles) samples. Red galaxies are defined as those no more than 0.15 mag bluer than a fit to the red sequence in $0.4(g-r)$, as shown in Figures 4 and 5. There is a significant excess of red galaxies in the group sample, at fixed luminosity.

tension of the blue sequence toward red ($g-i$) colours, but offset in ($i-K_s$) from the population of E and S0 galaxies, which show little or no activity. The solid lines show an approximate colour cut which isolates the population expected to be mostly inactive, from the more normally star-forming population. The same division is evident in the group sample, but now the inactive population is much more prominent.

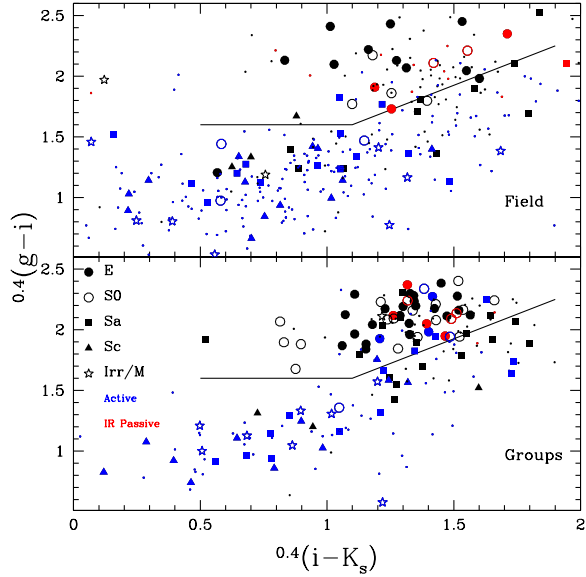


Figure 8. A colour-colour diagram for group (bottom) and field (top) galaxy populations. The y-axis is mostly sensitive to age, while the x-axis is more sensitive to dust. The passive, early-type population is well-separated from the more normal, active population, although they overlap in ($g-i$) colour. The solid lines show our choice for isolating the truly passive population, which lie to the left of these lines.

We therefore make our best attempt to identify galaxies which appear to be truly inactive. Our primary requirement for a passive galaxy is one that not only lies on the $0.4(g-r)$ red sequence defined above, but also shows colours typical of passively evolving galaxies in the $0.4(g-i)-0.4(i-K_s)$ diagram (Figure 8). We also remove from that sample any galaxy with strong [OII] emission ($W_\circ(O[II]) > 10\text{\AA}$), or an IR excess as measured from available *Spitzer* data (Section 3.4). This definition removes about 20 per cent of galaxies from the $0.4(g-r)$ red sequence, approximately independent of magnitude and environment. Most of this difference is due to the colour-selection; the additional contribution from [OII]-emitting or IR excess galaxies is relatively small.

Our best estimate of the truly inactive fraction is shown in Figure 9. The most important result here is that inactive galaxies are significantly more common in the group environment, at all magnitudes. Thus, the higher incidence of group galaxies on the ($g-r$) red sequence is not simply reflecting a dustier population. Secondly, in both environments, the fraction of inactive galaxies is only weakly dependent on M_{K_s} luminosity (closely related to stellar mass), though the large error bars on the most luminous points makes it difficult to draw strong conclusions.

Recall finally that our field sample consists of galaxies in all environments, including groups. In particular, approximately 40 per cent of our lowest-mass field galaxies, and 60 per cent of our highest mass field galaxies, are expected to be in groups or clusters (McGee et al. 2009). Using this, the fraction of “ungrouped”, inactive galaxies can be estimated from Figure 9. For example, at bright luminosities, 54 ± 6 per cent of group galaxies and 35 ± 3 per cent of field galaxies are inactive. Since $\sim 55 \pm 5$ per cent of the field galaxies themselves are expected to be in groups, this leaves room for only $\sim 11 \pm 15$ per cent inactive galaxies among the isolated component of our field sample. This is consistent with zero, for all luminosities considered here, suggesting that almost *all* of the

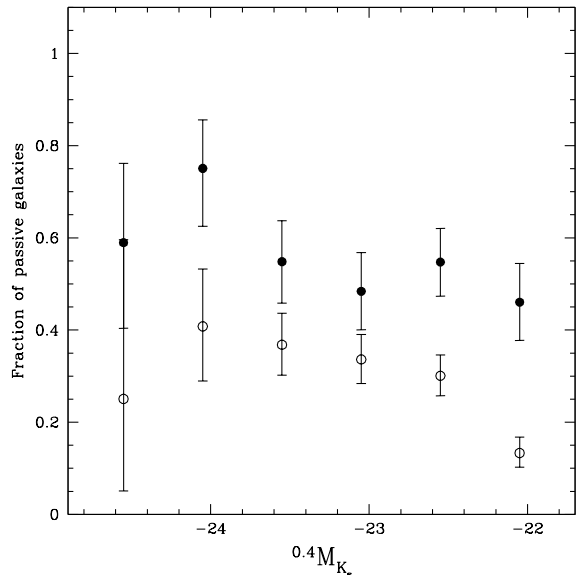


Figure 9. The fraction of galaxies identified as having no ongoing star formation from their $^{0.4}(g-i)-^{0.4}(i-K_s)$ colours as shown in Figure 8, and an absence of strong [OII] emission or an IR excess, if either of these indicators is available. Group galaxies are shown with filled circles, and the field with open circles. The field is a global sample, of which approximately 50 per cent are themselves in groups or clusters. Our data are consistent with isolated (or ungrouped) galaxies having few or no inactive galaxies whatsoever (see text for more details).

“red-and-dead” galaxies found in field surveys at this redshift are associated with dense environments.

4.3 Population Dynamics

We consider the dynamics of the different populations of group members, in Figure 10. This figure shows the velocity offset of every group member brighter than $^{0.4}M_i = -20.0$, relative to the velocity dispersion of the host group, as a function of distance from the group centre. Galaxies are divided into red-sequence and blue-cloud populations, based on their $^{0.4}(g-r)$ colours (Figure 4); green points denote red-sequence galaxies with some evidence of ongoing activity as described in § 4.2. Overall, the group population appears well separated from the surrounding field in velocity space, and evidence for overdense structure can be seen well beyond 1 Mpc (recall that all the analysis in this paper is restricted to the population within 0.5 Mpc). Secondly, the red and blue populations have very similar phase space distributions. Within 0.5 Mpc both appear to have a somewhat flatter velocity distribution than a Gaussian, although a Gaussian model cannot be ruled out with a Kolmogorov–Smirnov test. The similar dynamics of the two populations suggests that the blue galaxies are not preferentially contaminated by fore- and background galaxies.

Intriguingly, the red-sequence galaxies with evidence for ongoing star formation do exhibit some dynamical differences from the rest of the population. Those found within 0.5 Mpc have a velocity distribution statistically inconsistent (0.6% probability) with a Gaussian with a mean and dispersion given by the main galaxy population. The double-peaked distribution is characteristic of an infalling population; this may then represent a population in which star formation is being truncated upon first accretion into a group

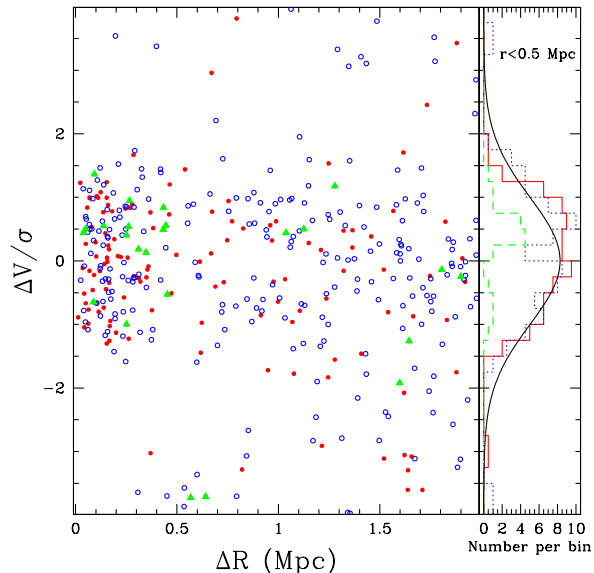


Figure 10. The rest-frame velocity offset, normalized to the group velocity dispersion, is shown as a function of physical distance from the group centre, for all galaxies with $^{0.4}M_i < -20.0$, near the groups in our sample. Galaxies are divided into red and blue populations (red, filled circles and blue, open circles, respectively) based on their gri photometry, as shown in Figure 4. Galaxies on the red sequence, but with evidence of activity, as discussed in § 4.2, are indicated with green triangles. The histograms on the right show the velocity distribution of each galaxy population, within 0.5 Mpc. The smooth, black curve is a Gaussian with unit variance and zero mean, normalized to match that of the observed, red galaxy population. Both the red (solid histogram) and the blue (dotted histogram) population are observed to have similar spatial and velocity distributions, somewhat flatter than a Gaussian. The “dusty red” galaxies (dashed histogram) shows a double-peaked distribution characteristic of infall.

environment. Whether or not this truncation is accompanied by a heavily obscured burst of star formation or not is unclear; we are currently analysing $24\mu\text{m}$ data from *Spitzer* that should shed light on this issue (Tyler et al. in prep).

5 DISCUSSION

We have shown that the optical colour distribution of group galaxies at $z \sim 0.4$ is very similar to that of the surrounding field, but with a more prominent population of red galaxies. While we cannot rule out a contribution from short-lived starbursts, or heavily dust-obscured star formation, we find no evidence that dense environments at this epoch are doing anything to *induce* star formation on a large scale. This is particularly relevant, since small groups are anticipated to be the prime environment for galaxy interactions to take place, and these interactions might lead to enhanced star formation. Furthermore, as galaxies in groups are destined to make up a substantial fraction of the massive cluster galaxy population by $z = 0$ (e.g. Berrier et al. 2009; McGee et al. 2009), it seems unlikely that the red population in clusters was produced via such starburst-inducing interactions within groups.

It is therefore useful to compare the group population with that of more massive galaxy clusters at a similar redshift. The most comparable survey is that of Ellingson et al. (2001), who have measured the blue fraction for fifteen massive clusters at

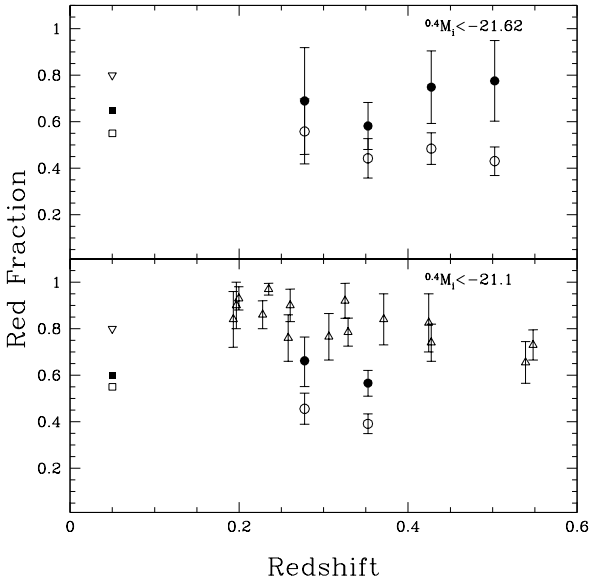


Figure 11. Bottom panel: The fraction of red galaxies brighter than $^{0.4}M_i = -21.1$, in our group (filled circles) and field (open circles) samples as a function of redshift. This is compared with the red fractions in X-ray luminous clusters over a similar redshift and luminosity range, shown as the open triangles, taken from Ellingson et al. (2001). We also show an estimate of the red fraction locally, from the SDSS sample of Weinmann et al. (2006a). The inverted triangles, filled and open squares represent clusters, groups and field galaxies, respectively. **Top panel:** Our full group and field sample, for a brighter luminosity limit of $^{0.4}M_i = -21.62$. The brighter limit allows us to plot consistent measurements for our sample over the full redshift range shown.

$0.3 < z < 0.5$, considering all galaxies within R_{200} brighter than $^{k,e}M_r = -20 - 5 \log h = -20.77$. At $z = 0.4$, the observed i magnitude corresponds very closely to rest-frame r , and is only about 0.1 mag fainter on average. We find our $z = 0.4$ i magnitudes, uncorrected for evolution, correspond to the magnitudes in Ellingson et al. (2001) approximately as

$$^{0.4}M_i \approx ^{k,e}M_r - 0.3 \pm 0.2 \quad (10)$$

Thus, to compare with the sample of Ellingson et al. (2001), we calculate the red fractions for galaxies brighter than $^{0.4}M_i = -21.1$, which corresponds approximately to a stellar mass limit of $2.8 \times 10^{10} M_\odot$. Our sample is only colour-complete to this limit for $z \leq 0.39$, so we restrict the analysis to these groups, and note that the clusters are probably also somewhat incomplete in red galaxies above this redshift, as the Ellingson et al. (2001) sample has a very similar selection function to ours. We do not know the masses of the groups well enough to estimate a robust value of R_{200} , but our radial selection of $r < 0.5$ Mpc is designed to be approximately this radius for the typical group in our sample; thus the comparison with the cluster data is fairly well-matched. The results are shown in Figure 11. The groups lie in an intermediate region of the diagram, between the field and the clusters. If we interpret the groups as an intermediate step in the hierarchical growth of clusters, this suggests that, with time, galaxies in dense environments slowly migrate onto the red sequence, perhaps via a stage where there is non-negligible star formation still occurring as inferred by Wolf et al. (2009).

We will defer a precise comparison with groups and clusters from different samples, over a wider range of redshifts, to a fu-

ture paper in which we present robust stellar mass estimates based on SED-fitting over the full spectrum from *GALEX*-UV to *Spitzer*-IR. However, in the meantime it is useful to make a crude comparison with luminosity-limited samples in the low-redshift Universe, and it is most straightforward to compare with the analysis of Weinmann et al. (2006a), based on the Yang et al. (2007) group catalogue from the SDSS. Using the above relation between $^{0.4}M_i$ and $^{k,e}M_r$, we estimate the corresponding red fraction in clusters (haloes with $M > 10^{14} M_\odot$), groups ($10^{13} > M/M_\odot > 10^{14}$) and the field (all galaxies). We include both the “early” and “intermediate” classifications of Weinmann et al. (2006a) in the red fraction, since these populations largely overlap in colour. These local red fractions are plotted as inverted triangles, filled squares, and open squares, respectively. Comparing the clusters with those of Ellingson et al. (2001), we see the well-known result that, at these relatively high stellar luminosities, there is little evolution in the cluster red fraction (e.g. Ellingson et al. 2001; Nakata et al. 2005; De Propriis et al. 2003). The same lack of evolution holds for the groups and even the field, which itself is dominated by galaxies within groups. This result is also in agreement with Balogh et al. (2004a), who find that for groups in the SDSS with $\sigma < 500$ km/s, the red fraction of galaxies with $M_r < -20$ is about 65%, very similar to the value obtained from the Weinmann et al. (2006a) analysis. This lack of evolution doesn’t come as a complete surprise, as evolution since $z = 1$ is largely dominated by the low-mass population, with $M \lesssim 3 \times 10^{10} M_\odot$ (e.g. Bell et al. 2007a).

5.1 Comparison with models

It has now been shown in several places that many simple models for galaxy formation predict too many faint, red satellite galaxies at low redshift. For example, Weinmann et al. (2006a) compare the SDSS data with model predictions from Croton et al. (2006), and show that real groups and clusters have a large population of faint, blue satellites that are almost completely absent in the models. This appears to be the result of an oversimplified gas-stripping model, whereby all hot gas is immediately removed from satellite galaxies upon merging with a larger halo. Recently, Font et al. (2008) have explored a more realistic model, based on the calculations of McCarthy et al. (2008). In this model, satellite galaxies are able to retain some fraction of their gas following accretion, depending on their orbit.

To compare with our data, we select field and group galaxies at $z = 0.4$ from both the Bower et al. (2006) and Font et al. (2008) models, using the algorithm described in McGee et al. (2008) to closely reproduce our observational selection criteria. In particular, group membership is determined from projected distances and line-of-sight velocities using the same friends-of-friends algorithm used to define the observed groups. We use the $z = 0.4$ observed-frame SDSS ($g-r$) colours and 2MASS K magnitude predicted by these models, to closely match the observed quantities we have presented here. In addition to the differences in gas-stripping physics, the Font et al. model has several other different parameter choices compared with the previous Bower et al. model, but these are of limited interest here. Our goal is to see how well the models reproduce the overall shape of the colour distribution, and we neglect statistical uncertainties on the magnitudes, which are relatively small.

In Figure 12, we show the colour histograms for both models, compared with our data. We focus only on the lowest luminosity galaxies for which our data are complete, $-22.25 < ^{0.4}M_k < -21.7$, since these are the most sensitive to environmental effects. Both models do a reasonable job at reproducing the observed bi-

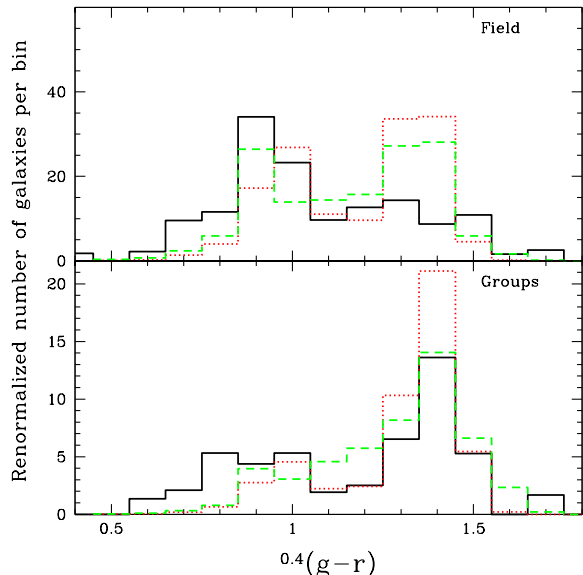


Figure 12. *Top panel:* The solid histograms show the observed $^{0.4}(g-r)$ colour distribution of galaxies in a narrow range of infrared luminosity, $-22.25 > ^{0.4}M_{K_s} > -21.7$, for our field sample. This is compared with the predicted colours from the models of Bower et al. (2006, red, dotted) and Font et al. (2008, green, dashed), where the group and field environments are defined in a way that is analogous to our observational selection. The observed distributions are statistically weighted, and all histograms are renormalized so their integrals reflect the total number of observed galaxies in the appropriate sample. *Bottom panel:* The same, but for our group samples.

modal colour distribution, but overpredict the fraction of galaxies in the red peak. Specifically, if we define red galaxies as those with $^{0.4}(g-r) > 1.2$ then the predicted red fraction in the field is 54% and 50% in the Bower and Font models, respectively, while the observed value is only $28 \pm 2\%$. Note that this discrepancy is not due to a mismatch in the near-infrared luminosity; the predicted red fractions change by only ~ 5 per cent within ± 0.5 mag of the luminosity range shown here.

Red, low-mass galaxies in these models are almost exclusively satellite galaxies for which the gas supply is assumed to have been lost. Thus, the group environment is expected to be the key that controls the overall fraction of red galaxies. In the bottom panel of Figure 12 we actually see a remarkably good qualitative agreement between the models and the observed colour distribution in groups. The older, Bower model predicts a red fraction 75%, still much too large compared with the observed $56 \pm 8\%$. The Font model achieves its goal of reducing this number, to 67%; however, it does so by overpopulating the “green valley” between the red and blue sequences. This is likely a consequence of adopting a slow strangulation timescale for every satellite galaxy; a better match might be achieved by only truncating star formation in a subset of galaxies, for example based on their orbital parameters. We will explore such an adjustment in a future paper.

Interestingly, both models predict that almost all of these blue “group” galaxies are found in haloes with $M < 1 \times 10^{12} M_{\odot}$; that is, they are nearby, but not actually incorporated into the main group halo. We therefore explore the dynamics of the galaxies

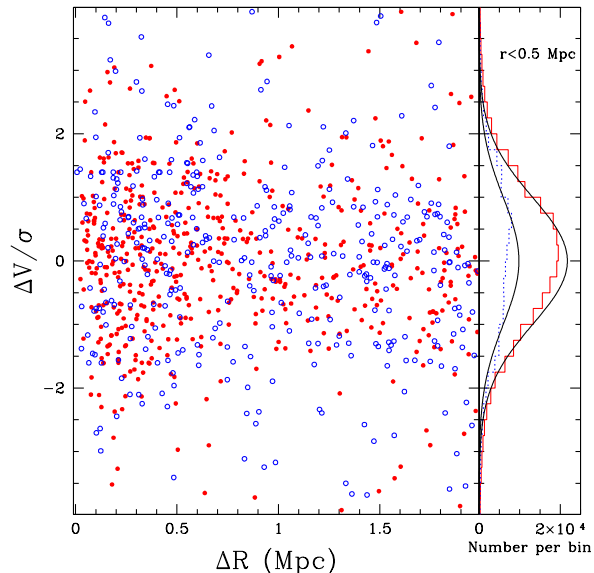


Figure 13. The equivalent of Figure 10 for the Font et al. (2008) model, this figure shows the velocity distribution as a function of projected distance for a sample of galaxies with $^{0.4}M_i < -20$ in the mock groups. The red points and histogram correspond to galaxies with $^{0.4}(g-r) > 1.2$, while the blue points represent bluer galaxies. In the left panel, only a random 0.13 per cent of the model predictions are shown; this yields a sample size comparable to that of our observations. In the right panel, Gaussian models with unit variance and zero mean are overplotted, normalized to the total area of the red and blue galaxy populations, for comparison. Both distributions are statistically distinct from Gaussians, and from each other. However, this distinction cannot be made if the sample size is reduced to match that of our observations.

in the Font model⁶ in Figure 13. This includes all galaxies with $^{0.4}M_i < -20$, and so can be compared directly with the observations from Figure 10. We first note that the blue population, despite arising from galaxies outside the main dark matter halo that defines the group, are clearly dynamically linked to the group. Therefore they are physically associated with the group, and not randomly projected field galaxies. Secondly, the distributions of both the red and blue populations are statistically inconsistent with a Gaussian, showing significantly flatter peaks. They are also statistically distinct from one another. However the difference is small, and if we choose a random subset of the model galaxies, so the sample size is comparable to that of our observational dataset, we can no longer statistically distinguish these distributions from a Gaussian. Therefore much larger data samples will be required to make use of these predictions.

6 CONCLUSIONS

We have presented an analysis of the optical and near-infrared properties of galaxies in small groups at $z = 0.4$. We measure colours consistently, using aperture photometry on *psf*-matched images, and minimize k-corrections by analysing the observations in the $z = 0.4$ frame. We use the optical $^{0.4}(g-r)$ colours, which bracket the 4000\AA break at this redshift, as our primary probe of the stellar

⁶ The results are similar if we consider the Bower et al. (2006) model instead.

population. Following Wolf et al. (2005) and Wilman et al. (2008) we also make use of the i photometry and *Spitzer* IRAC photometry, respectively, to distinguish dusty, star-forming galaxies from truly passive galaxies with red $^{0.4}(g-r)$ colours. Total luminosities are computed at near-infrared magnitudes, from *Spitzer*, *WHT* and *NTT* data; these can be related to the total stellar mass with relatively weak dependence on model assumptions.

We conclude the following:

- The group population contains a clear red-sequence of galaxies down to the lowest stellar mass for which we are complete, $M \approx 1 \times 10^{10} M_{\odot}$. This red sequence is populated mostly by galaxies with elliptical or S0 morphology. The most massive group galaxies, with $^{0.4}M_k < -23.5$ (corresponding to $M > 1 \times 10^{11} M_{\odot}$), are predominantly found on the red sequence.
- The fraction of galaxies in the red population depends on both near-infrared luminosity and environment. In all environments, the fraction of red galaxies decreases with decreasing luminosity, though the trend is relatively weak when near-infrared luminosities are used. Nonetheless, at all luminosities the fraction of red galaxies in groups is significantly larger than in the field, by $\sim 20 \pm 7$ per cent.
- In both the group and field samples, about 20 per cent of the optically-red galaxy population shows signs of dust-reddened star formation when longer wavelength photometry is considered. Accounting for this, 54 ± 6 per cent of the group population brighter than $^{0.4}M_k = -22$ is evolving passively. Only 35 ± 3 per cent of the field population is comprised of such galaxies, and this is consistent with the number expected if they were *only* found within groups and clusters (which are proportionally represented in our field sample).
- Considering fairly bright galaxies, $^{0.4}M_i \leq -21.1$, we compare our group galaxies to a similar sample of cluster galaxies, and find that the fraction of red galaxies is intermediate between that of the field (~ 40 per cent) and cluster (~ 80 per cent) populations.
- Including comparably-selected groups at $z \sim 0.05$ (Weinmann et al. 2006a; Balogh et al. 2004a), we detect no significant redshift evolution in the red fraction of the groups since $z < 0.55$, considering only the brightest galaxies for which we have a statistically complete sample, $^{0.4}M_i < -21.6$.

• The dynamics of the active and passive populations in the groups are not statistically distinguishable. The velocity distributions, though statistically consistent with Gaussian distributions, show some flattening (and bimodality in the blue and dusty-star forming population) characteristic of infall.

• The optical colour distribution of these groups is reasonably well-matched by the predictions of simple galaxy formation models, although the models overpredict the relative number of red (inactive) galaxies in groups. In particular, the Bower et al. (2006) model predicts a red fraction of 75%, considerably larger than the observed $56 \pm 8\%$. The more recent model of Font et al. (2008) tries to address this by increasing the timescale required for satellite quenching. While this model achieves a lower red fraction of 67%, it distorts the overall colour distribution, filling in the colour-space between the red and blue peaks in a way that is not seen in the observations.

In summary, galaxy groups at $z = 0.4$ appear to host galaxy populations that are intermediate in their star-formation history distribution, between that of the field and that of rich clusters at this redshift. This difference is characterised by a reduced fraction of galaxies of a given stellar mass undergoing current star formation activity, compared with the field. The colour distribution, and its

dependence on stellar mass and environment, is reasonably well reproduced by simple models that assume satellite galaxies lose their hot corona of gas on relatively short timescales. However, it remains an unsolved challenge to simultaneously match the red fraction and distinct bimodality of the galaxy colour distribution in different environments.

7 ACKNOWLEDGMENTS

We thank the GALFORM team for making their model predictions publicly available, and the CNOC2 team for allowing us to use their unpublished redshifts. We acknowledge useful conversations with Andreea Font, Ian McCarthy, David Gilbank, Mike Hudson, Frank van den Bosch and Simone Weinmann which helped to shape this work. We are also grateful to the anonymous referee, who made several suggestions which improved our analysis of these results. This work is based on observations made with: the *Spitzer* Space Telescope, operated by the Jet Propulsion Laboratory, California Institute of Technology, under a contract with NASA; the NASA/ESA Hubble Space Telescope, at the Space Telescope Science Institute, which is operated by the Association of Universities for Research in Astronomy, Inc., under NASA contract NAS 5-26555; the Canada-France-Hawaii Telescope, operated by the National Research Council (NRC) of Canada, the Institut National des Science de l'Univers of the Centre National de la Recherche Scientifique (CNRS) of France, and the University of Hawaii; the ESO telescopes at the La Silla Observatories, under programme ids 076.A.0346 and 077.A.0224; and the William Herschel Telescope, operated on the island of La Palma by the Isaac Newton Group in the Spanish Observatorio del Roque de Los Muchachos of the Instituto de Astrofísica de Canarias. This research made use of tools provided by astrometry.net, and the facilities of the Canadian Astronomy Data Centre, which is operated by the National Research Council of Canada with the support of the Canadian Space Agency. MLB acknowledges financial support from an NSERC Discovery Grant.

REFERENCES

- Baldry, I. K., Balogh, M. L., Bower, R. G., Glazebrook, K., Nichol, R. C., Bamford, S. P., & Budavari, T. 2006, *MNRAS*, 373, 469
- Baldry, I. K., Glazebrook, K., Brinkmann, J., Ivezić, Z., Lupton, R. H., Nichol, R. C., & Szalay, A. S. 2004, *ApJ*, 600, 681
- Balogh, M. L., Baldry, I. K., Nichol, R. C., Miller, C., Bower, R. G., & Glazebrook, K. 2004a, *ApJL*, 615, L101
- Balogh, M. L., Morris, S. L., Yee, H. K. C., Carlberg, R. G., & Ellingson, E. 1997, *ApJL*, 488, L75+
- . 1999, *ApJ*, 527, 54
- Balogh, M. L., Navarro, J. F., & Morris, S. L. 2000, *ApJ*, 540, 113
- Balogh, M. L. et al. 2004b, *MNRAS*, 348, 1355
- . 2007, *MNRAS*, 374, 1169
- Bamford, S. P., Milvang-Jensen, B., & Aragón-Salamanca, A. 2007, *MNRAS*, 378, L6
- Beers, T. C., Flynn, K., & Gebhardt, K. 1990, *AJ*, 100, 32
- Bell, E. F., Wolf, C., Meisenheimer, K., Rix, H., Borch, A., Dye, S., Kleinheinrich, M., Wisotzki, L., & McIntosh, D. H. 2004, *ApJ*, 608, 752
- Bell, E. F., Zheng, X. Z., Papovich, C., Borch, A., Wolf, C., & Meisenheimer, K. 2007a, *ApJ*, 663, 834

- Bell, E. F. et al. 2007b, *ApJ*, 663, 834
- Berrier, J. C., Stewart, K. R., Bullock, J. S., Purcell, C. W., Barton, E. J., & Wechsler, R. H. 2009, *ApJ*, 690, 1292
- Bertin, E. & Arnouts, S. 1996, *A&AS*, 117, 393
- Bildfell, C., Hoekstra, H., Babul, A., & Mahdavi, A. 2008, *MNRAS*, 389, 1637
- Birnboim, Y. & Dekel, A. 2003, *MNRAS*, 345, 349
- Blanton, M. R., Eisenstein, D., Hogg, D. W., Schlegel, D. J., & Brinkmann, J. 2005, *ApJ*, 629, 143
- Blanton, M. R. & Roweis, S. 2007, *AJ*, 133, 734
- Bower, R. G., Benson, A. J., Malbon, R., Helly, J. C., Frenk, C. S., Baugh, C. M., Cole, S., & Lacey, C. G. 2006, *MNRAS*, 370, 645
- Bruzual, G. & Charlot, S. 2003, *MNRAS*, 344, 1000
- Carlberg, R. G., Yee, H. K. C., Morris, S. L., Lin, H., Hall, P. B., Patton, D. R., Sawicki, M., & Shepherd, C. W. 2001a, *ApJ*, 563, 736
- . 2001b, *ApJ*, 552, 427
- Cassata, P. et al. 2008, *A&A*, 483, L39
- Chabrier, G. 2003, *PASP*, 115, 763
- Cole, S., Lacey, C. G., Baugh, C. M., & Frenk, C. S. 2000, *MNRAS*, 319, 168
- Cooper, M. C. et al. 2006, *MNRAS*, 370, 198
- . 2008, *MNRAS*, 383, 1058
- Cowie, L. L. & Barger, A. J. 2008, *ApJ*, 686, 72
- Crawford, C. S., Allen, S. W., Ebeling, H., Edge, A. C., & Fabian, A. C. 1999, *MNRAS*, 306, 857
- Croton, D. J. et al. 2006, *MNRAS*, 365, 11
- De Propris, R., Stanford, S. A., Eisenhardt, P. R., & Dickinson, M. 2003, *ApJ*, 598, 20
- Dekel, A. & Birnboim, Y. 2006, *MNRAS*, 368, 2
- Edwards, L. O. V., Hudson, M. J., Balogh, M. L., & Smith, R. J. 2007, *MNRAS*, 379, 100
- Eke, V. R. et al. 2004, *MNRAS*, 348, 866
- Elbaz, D. et al. 2007, *A&A*, 468, 33
- Ellingson, E., Lin, H., Yee, H. K. C., & Carlberg, R. G. 2001, *ApJ*, 547, 609
- Finn, R. A., Balogh, M. L., Zaritsky, D., Miller, C. J., & Nichol, R. C. 2008, *ApJ*, 679, 279
- Font, A. S. et al. 2008, *MNRAS*, 389, 1619
- Gallazzi, A. et al. 2009, *ApJ*, 690, 1883
- Gehrels, N. 1986, *ApJ*, 303, 336
- Gerke, B. et al. 2007, *MNRAS*, 376, 1425
- Gilbank, D. G. & Balogh, M. L. 2008, *MNRAS*, 385, L116
- Gilbank, D. G., Smail, I., Ivison, R. J., & Packham, C. 2003, *MNRAS*, 346, 1125
- Gomez, P. L., Nichol, R. C., et al. 2003, *ApJ*, 584, 210
- Gwyn, S. D. J. 2008, *PASP*, 120, 212
- Haines, C. P., Gargiulo, A., & Merluzzi, P. 2008, *MNRAS*, 385, 1201
- Haines, C. P., La Barbera, F., Mercurio, A., Merluzzi, P., & Busarello, G. 2006, *ApJL*, 647, L21
- Hogg, D. W., Blanton, M., Lang, D., Mierle, K., & Roweis, S. 2008, in *Astronomical Society of the Pacific Conference Series*, Vol. 394, *Astronomical Data Analysis Software and Systems XVII*, ed. R. W. Argyle, P. S. Bunclark, & J. R. Lewis, 27–
- Hsieh, B. C., Yee, H. K. C., Lin, H., & Gladders, M. D. 2005, *ApJS*, 158, 161
- Jarrett, T. H., Chester, T., Cutri, R., Schneider, S., Skrutskie, M., & Huchra, J. P. 2000, *AJ*, 119, 2498
- Jeltema, T. E., Mulchaey, J. S., Lubin, L. M., & Fassnacht, C. D. 2007, *ApJ*, 658, 865
- Juneau, S. et al. 2005, *ApJL*, 619, L135
- Kauffmann, G., Heckman, T. M., et al. 2003, *MNRAS*, 341, 54
- Koopmann, R. A. & Kenney, J. D. P. 2004, *ApJ*, 613, 866
- Lang, D., Hogg, D. W., Mierle, K., Blanton, M., & Roweis, S. 2009, in prep.
- Lewis, I. J. et al. 2002, *MNRAS*, 333, 279
- Marchesini, D., van Dokkum, P. G., Forster Schreiber, N. M., Franx, M., Labbe', I., & Wuyts, S. 2008, *ArXiv e-prints*
- McCarthy, I. G., Frenk, C. S., Font, A. S., Lacey, C. G., Bower, R. G., Mitchell, N. L., Balogh, M. L., & Theuns, T. 2008, *MNRAS*, 383, 593
- McGee, S. L., Balogh, M. L., Bower, R. G., Font, A., & McCarthy, I. 2009, *MNRAS*, submitted
- McGee, S. L., Balogh, M. L., Henderson, R. D. E., Wilman, D. J., Bower, R. G., Mulchaey, J. S., & Oemler, A. J. 2008, *MNRAS*, 664
- Moran, S. M., Ellis, R. S., Treu, T., Salim, S., Rich, R. M., Smith, G. P., & Kneib, J.-P. 2006, *ApJL*, 641, L97
- Muzzin, A., Wilson, G., Lacy, M., Yee, H. K. C., & Stanford, S. A. 2008, *ApJ*, 686, 966
- Nakata, F., Bower, R. G., Balogh, M. L., & Wilman, D. J. 2005, *MNRAS*, 357, 679
- O'Dea, C. P. et al. 2008, *ApJ*, 681, 1035
- Parker, L. C., Hudson, M. J., Carlberg, R. G., & Hoekstra, H. 2005, *ApJ*, 634, 806
- Pasquali, A., van den Bosch, F. C., Mo, H. J., Yang, X., & Somerville, R. 2009, *MNRAS*, 394, 38
- Poggianti, B. et al. 2006, *ApJ*, 642, 188
- Poggianti, B. M. et al. 2008, *ApJ*, 684, 888
- Rafferty, D. A., McNamara, B. R., & Nulsen, P. E. J. 2008, *ApJ*, 687, 899
- Schlegel, D. J., Finkbeiner, D. P., & Davis, M. 1998, *ApJ*, 500, 525
- Sijacki, D., Springel, V., di Matteo, T., & Hernquist, L. 2007, *MNRAS*, 380, 877
- Somerville, R. S., Hopkins, P. F., Cox, T. J., Robertson, B. E., & Hernquist, L. 2008, *MNRAS*, 1241
- Strateva, I., Ivezić, Ž., et al. 2001, *AJ*, 122, 1861
- Taylor, E. N. et al. 2009, *ApJ*, 694, 1171
- van den Bosch, F. C. et al. 2008, *MNRAS*, 387, 79
- Weinmann, S. M., van den Bosch, F. C., Yang, X., & Mo, H. J. 2006a, *MNRAS*, 366, 2
- Weinmann, S. M. et al. 2006b, *MNRAS*, 372, 1161
- Whitaker, R. 2005, PhD thesis, University of Durham
- White, S. D. M. & Frenk, C. S. 1991, *ApJ*, 379, 52
- Wilman, D. J., Balogh, M. L., Bower, R. G., Mulchaey, J. S., Oemler, A., Carlberg, R. G., Morris, S. L., & Whitaker, R. J. 2005a, *MNRAS*, 358, 71
- Wilman, D. J., Oemler, A., Mulchaey, J. S., McGee, S. L., Balogh, M. L., & Bower, R. G. 2009, *ApJ*, 692, 298
- Wilman, D. J. et al. 2005b, *MNRAS*, 358, 88
- . 2008, *ApJ*, 680, 1009
- Wolf, C., Gray, M. E., & Meisenheimer, K. 2005, *A&A*, 443, 435
- Wolf, C. et al. 2009, *MNRAS*, 128
- Yang, X., Mo, H. J., van den Bosch, F. C., Pasquali, A., Li, C., & Barden, M. 2007, *ApJ*, 671, 153
- Yee, H. K. C., Morris, S. L., Lin, H., Carlberg, R. G., et al. 2000, *ApJS*, 129, 475